Computational modeling establishes mechanotransduction as a potent entrainment cue for the mammalian circadian clock

E. A. Francis[1] and **P. Rangamani**[*1]

[1] *Department of Mechanical and Aerospace Engineering, University of California San Diego, CA 92093, USA*

Abstract

Mechanotransduction, which is the integration of mechanical signals from the cell's external environment to changes in intracellular signaling, governs many cellular functions. Recent studies show that the mechanical state of the cell is also coupled to the cellular circadian clock. To investigate possible interactions between circadian rhythms and cellular mechanotransduction, we developed a computational model that integrates these two pathways. Combining previous models of mechanotransduction and circadian clocks, we postulated that translocation of YAP/TAZ and MRTF into the nucleus leads to altered expression of circadian proteins. Simulations from our model predict that lower levels of cytoskeletal activity are associated with longer circadian oscillation periods and higher oscillation amplitudes, consistent with recent experimental observations. Furthermore, accumulation of YAP/TAZ and MRTF in the nucleus causes circadian oscillations to decay. These effects hold both at the single-cell level and within a population-level framework. Finally, we investigated the effects of mutations in YAP or lamin A, the latter of which lead to a class of diseases known as laminopathies. Oscillations in PER/CRY and BMAL1 are substantially weaker in populations of cells with *in silico* mutations in YAP and lamin A, suggesting that defects in mechanotransduction can disrupt the circadian clock in certain disease states. However, we find that normal oscillatory behavior can be rescued by lowering substrate stiffness, indicating a possible biological compensatory mechanism. Thus our study identifies that mechanotransduction could be a potent entrainment cue for cellular clocks and this crosstalk can be leveraged to rescue the circadian clock in disease states.

[*]To whom correspondence must be addressed: prangamani@ucsd.edu

Introduction

24 hour cycles known as circadian rhythms are a hallmark of life on earth. In mammals, organism-wide circadian oscillations are regulated by signals from the central circadian clock, located in the suprachiasmatic nucleus (SCN) of the hypothalamus [1, 2]. This central clock consists of a population of cells that exhibit oscillations in the expression of circadian proteins, including Brain and muscle Arnt-like protein-1 (BMAL1), Period (PER), Cryptochrome (CRY), and REV-ERBα [3, 4]. These oscillations are synchronized by environmental cues such as light-dark cycles via the process of entrainment. Remarkably, cells from peripheral tissues also exhibit 24-hour patterns of protein expression in these same circadian proteins even when removed from the body, demonstrating the intrinsic nature of the cellular circadian clock. Furthermore, these circadian cycles also regulate a wide range of functions in cells; for instance, about 43% of the mouse genome has been shown to undergo 24-hour cycles in transcription [5]. Recent experimental studies have revealed connections between disease states and disrupted circadian rhythms in different cell types [6, 7].

Local mechanical and chemical cues within a tissue may also serve as circadian clock regulators, providing a local form of clock entrainment [8]. While it has long been known that a serum shock synchronizes the circadian oscillations of cells in culture [9], it has recently been found that cytoskeletal activity also contributes to clock regulation [10, 11]. Additional studies have found that the circadian clock is mechanosensitive – the strength of oscillations changes depending on substrate stiffness [12, 13]. Xiong *et al.* recently analyzed this phenomenon in detail, demonstrating that altering the mechanical state of fibroblasts or U2OS cells by either treating with actomyosin inhibitors or seeding cells on substrates of different stiffnesses leads to distinct changes in the period and amplitude of circadian oscillations [14]. In particular, decreases in cytoskeletal activity were generally associated with increases in PER2 oscillation period and amplitude. This was shown to depend on myocardin-related transcription factor (MRTF)-dependent activation of serum response factor (SRF) in the nucleus. In a different study, Abenza *et al.* found that increased levels of yes-associated protein (YAP) and PDZ-binding motif (TAZ) in the nucleus correlated with significant perturbations to circadian oscillations in fibroblasts [15]. This effect was at least partially mediated by transcriptional enhanced associate domain (TEAD). Together, these findings suggest that the cell circadian clock can be affected by the key players in cellular mechanotransduction *viz.* MRTF and YAP/TAZ.

The nuclear translocation of transcriptional regulators such as YAP/TAZ and MRTF is a critical downstream event in cellular mechanotransduction, in which cells respond to their mechanical environment via force-dependent changes in biochemical signaling networks. For instance, cells on stiffer substrates show increased levels of focal adhesion kinase (FAK) phosphorylation, leading to down-

stream changes in cytoskeletal activity and nuclear localization of YAP/TAZ and MRTF. YAP/TAZ and MRTF then bind transcription factors such as TEAD and SRF, causing changes in gene expression. Accordingly, tissue stiffness is a critical determinant of cell behavior, controlling processes from stem cell differentiation to cell migration [16]. Additionally, changes to tissue stiffness are often observed in diseases such as cancers, likely contributing to their pathophysiologies [17]. Here, we examine how changes in tissue stiffness or other mechanical factors might disrupt the circadian clock, perhaps contributing to certain cases of disease progression.

How might cell signaling due to mechanotransduction and circadian oscillations be connected? In this study, we sought to answer this question using computational modeling. Building on the rich history of modeling circadian oscillations in single cells [18–20] and independent models of stiffness-dependent mechanotransduction [21, 22], we developed a model of mechanotransduction-induced perturbations to the cell circadian clock. We constrained our model to recently published experiments, and then used it to investigate the coupling between cell signaling and circadian oscillations in single cells and populations of cells. Finally, we investigated how mutations in YAP or lamin A might impact circadian oscillations. We found that such mutations can significantly weaken circadian oscillations, but this effect can be counteracted by reductions in substrate stiffness. Our model has implications for laminopathies, a class of diseases marked by mutations in the gene for lamin A, as well as diseases marked by changes in local tissue stiffness.

Results

Model development

We developed a mathematical model that includes YAP/TAZ and MRTF-mediated mechanotransduction as well as circadian oscillations in the expression of BMAL1 and PER/CRY proteins (Figure 1A). The process of mechanosensing leading to nuclear translocation of YAP/TAZ and/or MRTF occurs at a faster timescale compared to changes in the expression of circadian proteins (Figure 1B) and is assumed to remain constant over several days. Accordingly, we compute nuclear YAP/TAZ and MRTF steady-state values and use these as inputs to the dynamical model of circadian oscillations. Furthermore, in all cases, we assume that species are well-mixed within a given cellular compartment (plasma membrane, cytosol, nuclear membrane, or interior of the nucleus), allowing us to treat these systems using ordinary differential equations (ODEs) and delay differential equations (DDEs). We briefly summarize the mechanotransduction and circadian clock sections of the model below.

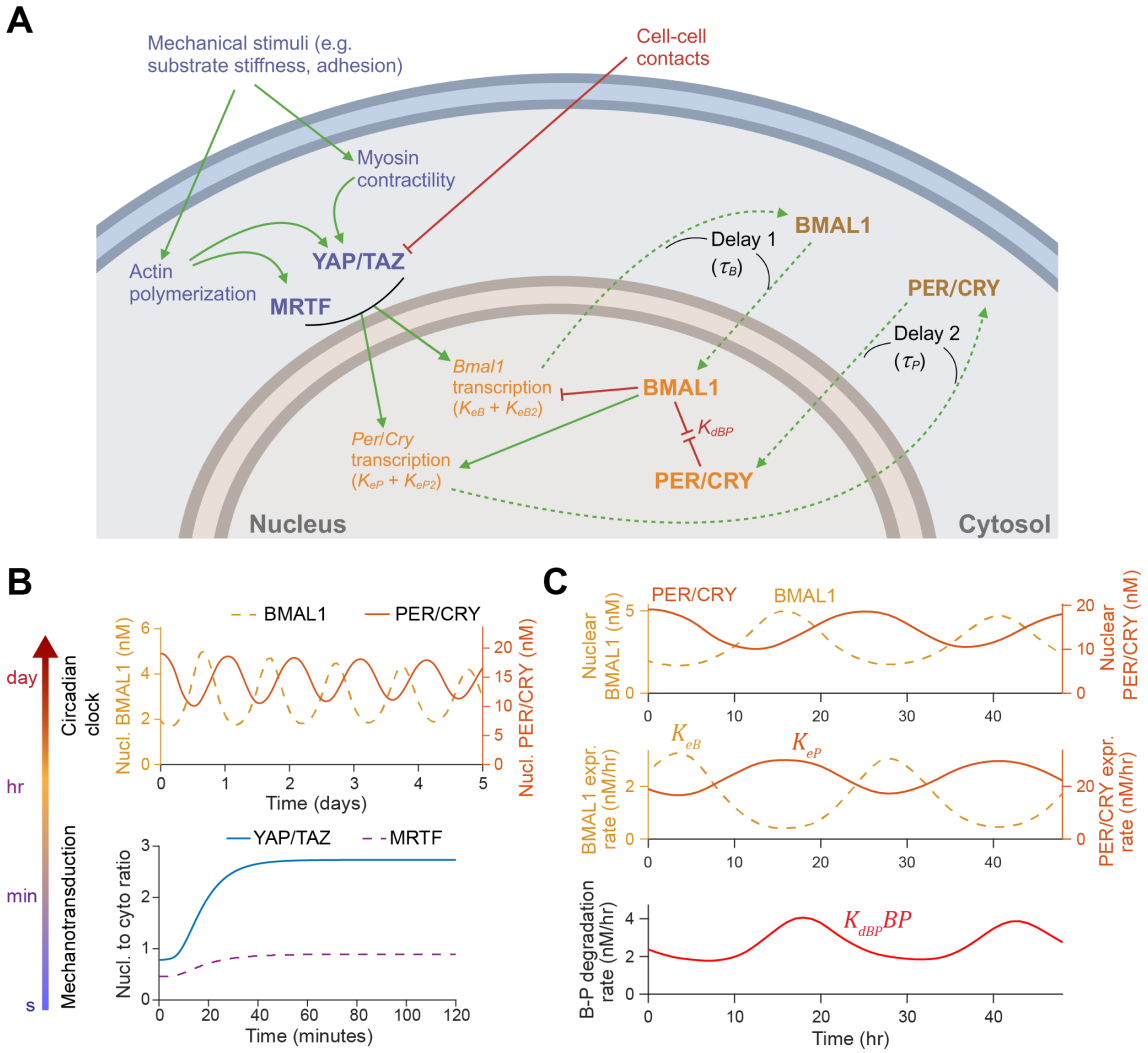

Figure 1: A coupled model of mechanotransduction and the circadian clock. (cont. on next page)

Figure 1: (cont. from previous page.) A) Schematic of pathways for YAP/TAZ and MRTF-mediated mechanotransduction and the mammalian circadian clock. Mechanical stimuli such as substrate stiffness and cell-substrate adhesion induce changes in cytoskeletal activity that lead to nuclear translocation of YAP/TAZ and MRTF. Cell-cell contacts also inhibit YAP/TAZ activation via a LATS-dependent pathway. Nuclear YAP/TAZ and MRTF are posited to induce changes in the expression of BMAL1, PER, and CRY proteins, altering circadian oscillations. In parallel, increases in nuclear BMAL1 inhibit transcription of the *Bmal1* gene and enhance transcription of *Per* and *Cry*. Dashed lines indicate delays associated with transcription, translation, post-translational modifications, and nuclear translocation of BMAL1 and PER/CRY. Parameters from Equations (5) and (6) are included with their associated reactions for clarity. The schematic was created with Biorender.com. B) Separation of timescales from mechanotransduction pathways to circadian oscillations. Events downstream of mechanical stimuli lead to changes in YAP/TAZ and MRTF nuclear concentrations within tens of minutes (lower plot), whereas changes in the concentration of circadian proteins are extended over hours to days (upper plot). C) Simulated dynamics of single-cell circadian oscillations. PER/CRY and BMAL1 both oscillate with periods close to 1 day and are out-of-phase with one another. Rates of expression of each gene and degradation of the PER/CRY-BMAL1 complex are depicted in lower plots.

YAP/TAZ and MRTF mechanotransduction model

Our mechanotransduction model is built from the model originally developed by Sun *et al.* [21] and then expanded by Scott *et al.* [22]. In brief, cell-substrate adhesion leads to substrate-stiffness dependent phosphorylation of focal adhesion kinase (FAK) adjacent to the cell membrane, triggering downstream activation of the GTPase RhoA. RhoA then activates both Rho kinase (ROCK) and mDia, which promote myosin activity and actin polymerization, respectively. ROCK also indirectly promotes actin polymerization by activating LIM kinase (LIMK), which inactivates cofilin, an F-actin-severing protein. Upon activation, myosin and actin form stress fibers, leading to the dephosphorylation of YAP and TAZ in the cytosol and allowing their translocation into the nucleus. When simulating different cell densities, we also assume that cell-cell contacts can induce increased phosphorylation of YAP/TAZ via a LATS-dependent pathway, causing more YAP/TAZ to remain cytosolic. Actin polymerization also permits the release of G-actin-sequestered MRTF, which can then translocate into the nucleus. As in [22], we assume that transport of YAP/TAZ into the nucleus depends on the phosphorylation state of lamin A; in particular, lamin A is increasingly dephosphorylated on stiffer substrates, leading to its incorporation into the nuclear lamina and concomitant stretching of the nuclear pore complex (NPC) [23]. This allows for increased transport of both YAP/TAZ and MRTF into the nucleus. In [22], MRTF was not included; whereas in [21], contributions of lamin A and the NPC to the nuclear transport of MRTF and YAP/TAZ were not considered. Here, we combine elements of both models to fully examine both YAP/TAZ and MRTF nuclear translocation. This mechan-

otransduction model includes 25 species, which can be reduced to 13 ordinary differential equations by mass conservation. In this case, we solve for steady state values by setting each differential equation equal to zero; the resulting expressions for each steady-state quantity are given in Table S1. For all YAP/TAZ-related parameters, we use the values previously estimated for mammalian cells in [22] (see Table S2), and MRTF-specific parameters and sensitivities to different treatment conditions were calibrated as described below. Baseline values for MRTF rate constants were set to match the values used for YAP/TAZ in [22] where applicable (Table 1).

Table 1: Estimated MRTF mechanotransduction and inhibitor treatment parameters.

Parameter	Units	Description	Baseline	Source	Fitting range (%)	MAP
$K_{in,solo,MRTF}$	1	MRTF nuclear entry rate constant	1	[22]	25-400	2.708
$K_{in,2,MRTF}$	μm^2	Lamin-A-dependent MRTF nuclear entry rate constant	10	[22]	25-400	8.500
$K_{release,MRTF}$	μM	Binding affinity of MRTF to G-actin	100	*	25-400	208.4
$C_{stiffness}$	kPa	Threshold stiffness for FAK phosphorylation	3.25	[22]	25-400	12.86
$K_{cap,CytD}$	μM	Cytochalasin D binding affinity for F-actin capping	2	†	25-400	6.268
$K_{dim,CytD}$	μM	Cytochalasin D binding affinity for G-actin dimerization	2	†	25-400	1.235
K_{Y27632}	μM	Y27632 treatment EC50	10	†	25-400	19.10
K_{LatB}	μM	Latrunculin B treatment EC50	0.2	†	25-400	0.1915
$K_{1,Jas}$	1	Jasplakinolide treatment constant 1	2	[24] ‡	25-400	2.277
$K_{2,Jas}$	μM	Jasplakinolide treatment constant 2	0.1	[24] ‡	25-400	0.03780

Fitting range specifies the range of the uniform prior distribution (in percentage) and "MAP" is the maximum *a posteriori* from Bayesian parameter estimation.

* $K_{release,MRTF}$ initialized to a moderate value of G-actin based on the total amount of actin in the cell.

† Moderate treatment concentrations used in [14].

‡ Baseline values approximated from observed effects *in vitro*; see Fig 4 in [24]

Circadian clock model

There is a vast body of literature on modeling cell circadian oscillations (reviewed in [18]). Here, rather than attempt to recapitulate the mammalian circadian clock in full mechanistic detail, we develop a minimal model, including the dynamics of negative clock regulators and positive clock regulators through two representative species, B (BMAL1) and P (PER and CRY proteins). This reduced approach is made possible by using delay differential equations (DDEs), as in multiple previous circadian models [20, 25, 26]. The relationships used in our model are primarily motivated by the

single DDE model used in [20] and the more detailed ODE model used in [19].

In our model, BMAL1 inhibits its own expression after translocating into the nucleus and forming a complex with CLOCK (circadian locomotor output cycles kaput). CLOCK levels remain relatively constant over time [27], and so it is not treated as a separate dynamical variable here. We note that this self-inhibition is indirect in reality, ultimately mediated by REV-ERBα [3]. This effect is modeled as an inhibition with delay τ_B, which represents the time between changes in transcription and associated changes in the nuclear concentration of BMAL1. This includes the time for transcription, translation, post-translational modifications, and shuttling of BMAL1 into the nucleus. As a starting estimate for this, we use the time gap between peak BMAL1 transcription and peak nuclear BMAL1, which has been measured at 12-16 hours in mouse fibroblasts [28]. Writing $B[t-\tau_B]$ as the nuclear concentration of B at time $t-\tau$, we express the self-regulated BMAL1 expression level as:

$$K_{eB}[t-\tau_B] = \frac{K_{eB0}}{1+\left(\frac{B[t-\tau_B]}{K_{iB}}\right)^2}. \tag{1}$$

Similarly, BMAL1 positively regulates the expression of negative clock elements (PER/CRY, or P here). Writing the delay between changes in PER/CRY transcription and eventual changes in nuclear PER/CRY as τ_P (approximated to be 6-9 hours based on measurements in mouse cells [29–31]), the BMAL1-regulated expression of PER/CRY is:

$$K_{eP}[t-\tau_P] = \frac{K_{eP0}}{1+\left(\frac{K_{aP}}{B[t-\tau_P]}\right)^2}. \tag{2}$$

We assume that nuclear YAP/TAZ ($[Y_{nuc}]$) and MRTF ($[M_{nuc}]$) independently regulate the expression of BMAL1 and PER/CRY via TEAD and SRF, respectively. In reality, these processes may not be fully independent of the nuclear concentrations of BMAL1 and PER/CRY, but sufficient mechanistic details are not available to justify a particular functional dependence. These YAP/TAZ and MRTF-dependent expression terms, K_{eB2} and K_{eP2} are written in the following general form:

$$K_{eB2} = K_{eB2,Y}\frac{[Y_{nuc}]^2}{[Y_{nuc}]^2+K_{YB}^2} + K_{eB2,M}\frac{[M_{nuc}]^2}{[M_{nuc}]^2+K_{MB}^2}, \tag{3}$$

$$K_{eP2} = K_{eP2,Y}\frac{[Y_{nuc}]^2}{[Y_{nuc}]^2+K_{YP}^2} + K_{eP2,M}\frac{[M_{nuc}]^2}{[M_{nuc}]^2+K_{MP}^2}. \tag{4}$$

It should be noted that $[Y_{nuc}]$ and $[M_{nuc}]$ in Equations (3) and (4) are steady-state values; it is implicitly assumed that the mechanotransduction signaling pathways have reached steady state prior

to the start of our simulations. If we were to consider YAP/TAZ and MRTF dynamics, these terms would be subject to the same delays as K_{eB} and K_{eP}.

In addition to these sources of regulation, PER/CRY proteins provide negative feedback by binding to and deactivating the BMAL1-CLOCK complex in the nucleus, as in [19]. We write out the full set of DDEs, including this BMAL1-PER/CRY interaction and decay terms for each species individually:

$$\frac{dB}{dt} = K_{eB}[t - \tau_B] + K_{eB2} - K_{dBP}BP - K_{dB}B, \tag{5}$$

$$\frac{dP}{dt} = K_{eP}[t - \tau_P] + K_{eP2} - K_{dBP}BP - K_{dP}P. \tag{6}$$

For a direct comparison of our model to experimental measurements of luminescence from cells expressing a PER2 promoter-driven luciferase reporter (PER2::Luc) [14, 32], we explicitly modeled luciferase dynamics. Assuming the expression of luciferase scales directly with PER2 expression and luciferase decays with rate K_{dL}, its dynamics are given by integrating the following expression:

$$\frac{dL}{dt} = K_{eP}[t - \tau_L] + K_{eP2} - K_{dL}L. \tag{7}$$

Altogether, this system involves 18 free parameters and 2 fixed values as summarized in Table 2. Baseline values were chosen to match the single DDE system in Lema *et al.* [20], experimentally measured delays [28–31], or were empirically set from early testing of the model.

Sensitivity analysis and model calibration

We assessed model sensitivity to each parameter by computing the total-order Sobol indices associated with the luciferase reporter's oscillation period and amplitude (Figure 2A-B). The oscillation period shows a moderate to strong dependence on all parameters tested. In general, the parameters associated with BMAL1 dynamics are stronger determinants of luciferase period, despite the fact that luciferase expression is directly coupled to PER/CRY expression. This demonstrates the predominant influence of BMAL1 as the driver of oscillations in our model via time-delayed negative feedback. The oscillation period is most sensitive to $K_{eB2,Y}$ among the mechanotransduction-circadian coupling parameters, indicating that YAP/TAZ may be a stronger regulator of circadian oscillations than MRTF in our model. Unsurprisingly, luciferase oscillation amplitude is most sensitive to $K_{d,Luc}$, the degradation rate of luciferase in the cytosol. K_{aP} and K_{eP0} play a secondary role in determining oscillation amplitude by controlling the magnitude of PER/CRY expression.

Table 2: Circadian clock model parameters.

Parameter	Units	Description	Baseline	Source	Fitting range (%)	MAP
τ_B	hr	BMAL1 delay constant	12.0	[28]	80-120	12.97
K_{eB0}	hr^{-1}	BMAL1-dependent BMAL1 expression rate	1.0	[20]	25-400	2.241
K_{iB}	1	Inhibition constant for BMAL1 expression	0.04	[20]	25-400	0.04332
K_{dBP}	hr^{-1}	PER/CRY/BMAL1 complex degradation rate	1.0	*	25-400	0.8673
K_{dB}	hr^{-1}	BMAL1 degradation rate	0.4	[20]	25-400	0.3314
τ_P	hr	PER/CRY delay constant	7.5	[29–31]	25-400	7.742
K_{eP0}	hr^{-1}	BMAL1-dependent PER/CRY expression rate	1.0	*	25-400	2.476
K_{aP}	1	Activation constant for PER/CRY expression	0.5	*	25-400	0.1253
K_{dP}	hr^{-1}	PER/CRY degradation rate	0.4	*	25-400	1.525
$K_{eB2,Y}$	hr^{-1}	YAP/TAZ-regulated BMAL1 expression rate	0.05	*	25-400	0.1626
K_{YB}	nM	Activation constant for YAP/TAZ regulation of BMAL1 expression	1.0	*	25-400	0.7269
$K_{eB2,M}$	hr^{-1}	MRTF-regulated BMAL1 expression rate	0.05	*	25-400	0.06452
K_{MB}	nM	Activation constant for MRTF regulation of BMAL1 expression	1.0	*	25-400	2.315
$K_{eP2,Y}$	nM hr^{-1}	YAP/TAZ-regulated PER/CRY expression rate	0.05	*	25-400	0.08432
K_{YP}	nM	Activation constant for YAP/TAZ regulation of PER/CRY expression	1.0	*	25-400	1.883
$K_{eP2,M}$	nM hr^{-1}	MRTF-regulated PER/CRY expression rate	0.05	*	25-400	0.09955
K_{MP}	nM	Activation constant for MRTF regulation of PER/CRY expression	1.0	*	25-400	1.770
$K_{d,Luc}$	hr^{-1}	Luciferase degradation rate	0.35	[33]	25-400	0.5461
τ_L	hr	Luciferase delay constant	1	**	**	1
C_{ref}	nM	Reference concentration	13.5	†	†	13.5

Table 2: (cont. from previous page) Fitting range specifies the range of the uniform prior distribution (in percentage) and "MAP" is the maximum *a posteriori* from Bayesian parameter estimation.
* Set based on early testing of the model, such that oscillations still occur when carrying over applicable parameter values from [20].
** The choice of τ_L is arbitrary in this equation; it does not affect model behavior, as it simply sets the phase of luciferase oscillations, but changes in luceriferase do not feedback to affect any other dynamics.
† To convert dimensionless PER/CRY and BMAL1 concentrations to nM, we multiplied these concentrations by C_{ref}. We set this parameter to 13.5 nM to match with experimental measurements which place the peak PER2 nuclear concentration at about 20 nM [34]. C_{ref} is fixed and not used in fitting as our fitting protocol only examines relative changes in nuclear concentration (see Supporting Information).

Because the circadian oscillation period was sensitive to all parameters, we sought to estimate each parameter rather than use arbitrary default values. Given the inherent variability in biological systems, we estimated probability distributions rather than point estimates for all parameters in Table 1 and Table 2 using Bayesian parameter estimation [35]. We utilized measurements of PER2::Luciferase mouse primary fibroblasts in Xiong *et al.* [14] to calibrate our model. We minimized the error between model predictions and experimental measurements for circadian oscillations after changing substrate stiffness (Figure 2C) or treating cells with ROCK inhibitor (Y27632) (Figure 2D), cytochalasin D (Figure 2E), latrunculin B (Figure 2F), or jasplakinolide (Figure 2G). These treatments introduce distinct effects on the cytoskeleton or associated signaling pathways while only introducing five additional free parameters. Overall, simulations using parameters sampled from their posterior distributions (Figure S1) provided a reasonable fit to experimental data (Figure 2C-G, Figure S2). We note that although our model does not capture the full dramatic decrease in oscillation period upon jasplakinolide treatment in [14] (Figure 2G), it does recapitulate the qualitative behavior of rapidly decaying oscillations at high jasplakinolide concentrations. More details on sensitivity analysis and parameter estimation are given in Methods (Section "Sensitivity analysis and parameter estimation") and Supporting Information (Section S3).

Mechanical factors alter the stability and dynamics of circadian oscillations

We examined the behavior of our model using the set of maximum *a posteriori* parameters from Bayesian parameter estimation (Tables 1 and 2). This corresponds to a single representative cell that exhibits behavior close to the mean population measurements from [14].

We first tested the effects of changing substrate stiffness. F-actin, cytosolic stiffness, nuclear YAP/TAZ, and nuclear MRTF all increase consistently as a function of substrate stiffness (Figure 3A), matching well with experimentally measured trends (e.g., see Figure S3). In turn, we observed marked changes to circadian oscillations (Figure 3B); as substrate stiffness increases, the period and amplitude of circadian oscillations also increase, but the overall oscillatory nature remains consistent. These find-

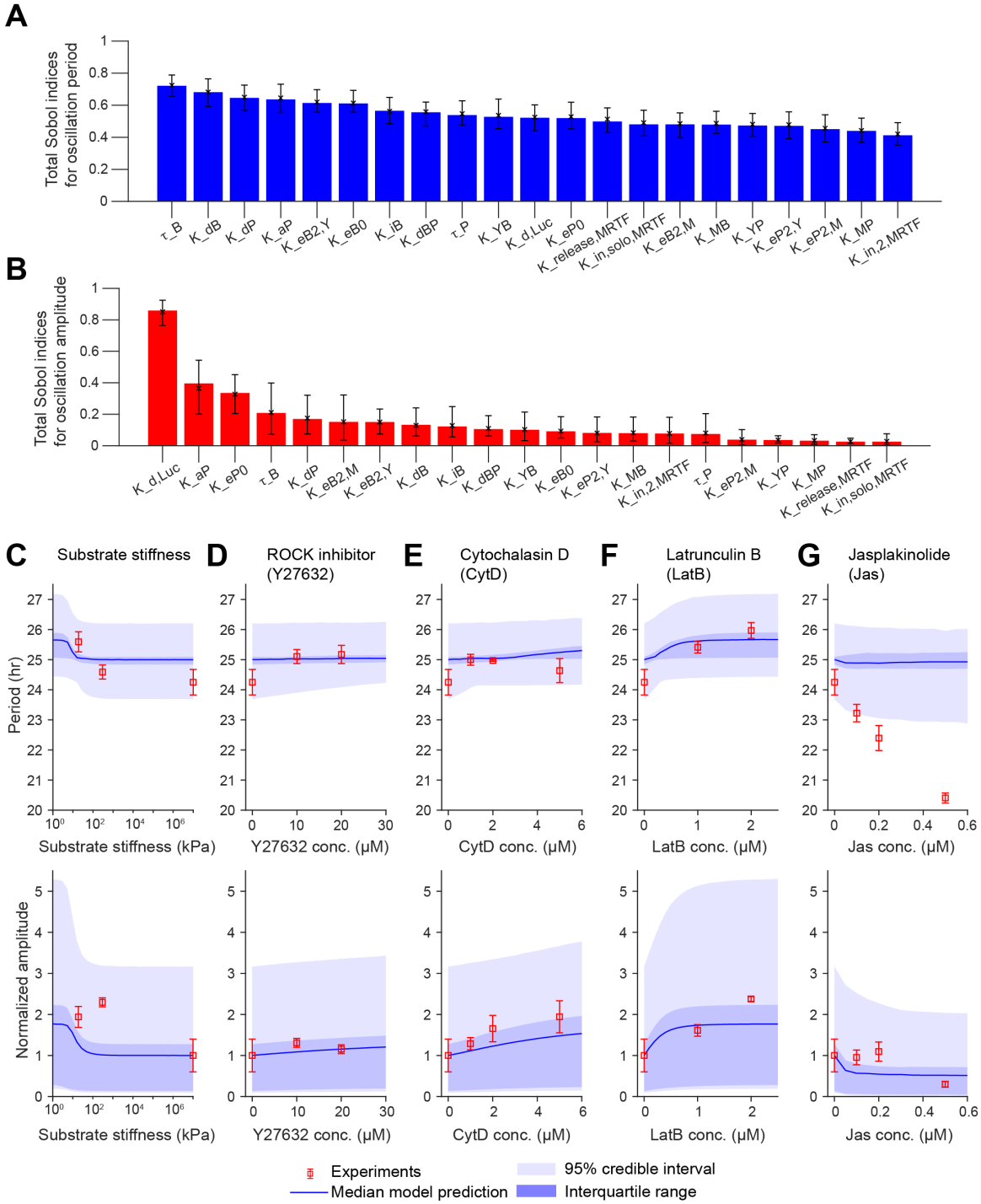

Figure 2: Global sensitivity analysis and Bayesian parameter estimation. (cont. on next page)

Figure 2: (cont. from previous page.) A-B) Total Sobol indices associated with the luciferase oscillation period (A) and amplitude (B). In each case, parameters are ordered from the highest to the lowest Sobol index. Sobol indices were computed with a sample size of 1000 and error bars denote 95% confidence intervals computed from bootstrapping with 100 replications. C-G) Predicted oscillation period and amplitude in 5 experiments from Bayesian parameter estimation. Experimental data from Xiong *et al.* [14] and model values are plotted for the effects of substrate stiffness (C), ROCK inhibitor (Y27632) treatment (D), cytochalasin D treatment (E), latrunculin B treatment (F), and jasplakinolide treatment (G). Experimental error bars denote standard deviation. For the model, the darker blue region indicates interquartile range and the lighter blue region spans the 95% credible interval (region from the 2.5 percentile to 97.5 percentile), based on sampling from the posterior distributions for parameter values. 1000 samples were generated to compute the estimates in this figure.

ings agree well with the data used for model calibration [14] and validate the coupling between our mechanotransduction module and the circadian module.

Next, we investigated how two different cytoskeleton-targeting drugs, cytochalasin D and jasplakinolide, affect circadian oscillations. Cytochalasin D is known to act by capping existing actin filaments and inducing dimerization of G-actin. We modeled this in a similar manner to [36], as fully described in Supporting Information (Section S2.1, Table S3). Because cytochalasin D treatment decreases the concentration of both F-actin and G-actin, it induces opposite effects on nuclear YAP/TAZ and MRTF (Figure 3C). Specifically, nuclear YAP/TAZ decreases whereas nuclear MRTF increases due to the G-actin dimerization, in agreement with experiments [37, 38]. Jasplakinolide stabilizes actin filaments and also induces polymerization [24]. We modeled this by assuming that the polymerization rate increases and the depolymerization rate decreases as a function of jasplakinolide concentration ((Section S2.3, Table S3)). As a result, F-actin accumulates in the cytosol, leading to increased levels of YAP/TAZ and MRTF in the nucleus (Figure 3E).

As expected, these inhibitor treatments have distinct effects on circadian oscillations. Similar to the effects of lower substrate stiffness, cytoskeletal inhibition by cytochalasin D leads to increased circadian oscillation period and amplitude (Figure 3D). Conversely, when actin polymerization is enhanced via jasplakinolide treatment, YAP/TAZ and MRTF accumulate in the nucleus, leading to a slight decrease in oscillation period and rapidly decaying oscillations (Figure 3F). Together, these simulations suggest that circadian oscillations are robust at lower levels of nuclear YAP/TAZ and MRTF, but upon accumulation of these factors in the nucleus, oscillations can decay over time. The location of this transition from stable to decaying oscillations (the Hopf bifurcation) in the YAP/TAZ-MRTF plane is shown in Figure 3G.

This general behavior, in which a Hopf bifurcation occurs for higher nuclear concentrations of YAP/TAZ and MRTF, is not exclusive to the single set of parameters used here. This feature of the model is

conserved for wide range of K_{dBP}, K_{dB}, and K_{dP} tested in Figure S4. In fact, even a further reduced version of our model (analyzed analytically in Supporting Information) shows this same trend: sustained circadian oscillations only occur when mechanically induced expression remains below a certain threshold. For many combinations of parameter values, we find that the line demarcating the bifurcation is close to vertical, indicating that nuclear YAP/TAZ is often the stronger determinant of stability compared to nuclear MRTF. Similarly, across almost all cases, changes in oscillation period occur mainly as a function of nuclear YAP/TAZ (that is, lines of constant period are nearly vertical). This agrees well with the finding that oscillation period is highly sensitive to the coupling strength between YAP/TAZ and BMAL1 expression (Figure 2A). Thus, our model predicts that while YAP/TAZ and MRTF both influence circadian oscillations, YAP/TAZ may be a more potent regulator of the circadian clock.

Model captures population-level variability in circadian oscillations

We next sought to capture population-level variability in circadian oscillations in our model. To incorporate population-level features, we focused on intercellular variation of kinetic parameters. Taking inspiration from computational studies in cardiomyocytes [39, 40] and stochastic models of genetic oscillators [41], we represented this natural variability in kinetic parameters by generating a model cell population in which individual cells have kinetic parameters drawn from probability distribution functions. These distributions were either assumed to be log-normal or were directly adopted from the posterior distributions derived from Bayesian parameter estimation (Section "Simulation of cell populations", Figure S1) to represent a range of statistically likely parameter sets. Furthermore, to capture additional sources of measurement noise, we added Gaussian white noise to each time series after solving the DDEs.

We first verified that simulations using this modified model still captured the overall trends seen at the single-cell level (Figure 3) while displaying increased variability. In this case, we analyze oscillations in BMAL1 rather than PER/CRY for a more direct comparison with the population-level data from Abenza *et al.* [15] (see justification in Methods, Section "Calculation of the circadian power fraction"). Plotting population BMAL1 dynamics as a kymograph, we observe that circadian oscillations appear to be stronger on a soft substrate compared to cells on glass (Figure 4A-B), similar to the decreased oscillation amplitude observed on stiff substrates in the single-cell case (Figure 3A). In further agreement with single-cell observations, cells on stiffer substrates exhibit decreased oscillation period on average (Figure 4C).

To quantify the overall disruption to circadian oscillations, we used a metric called the circadian power fraction (originally defined in [15]), which ranges from 0 (no circadian oscillations) to 1 (perfect sinu-

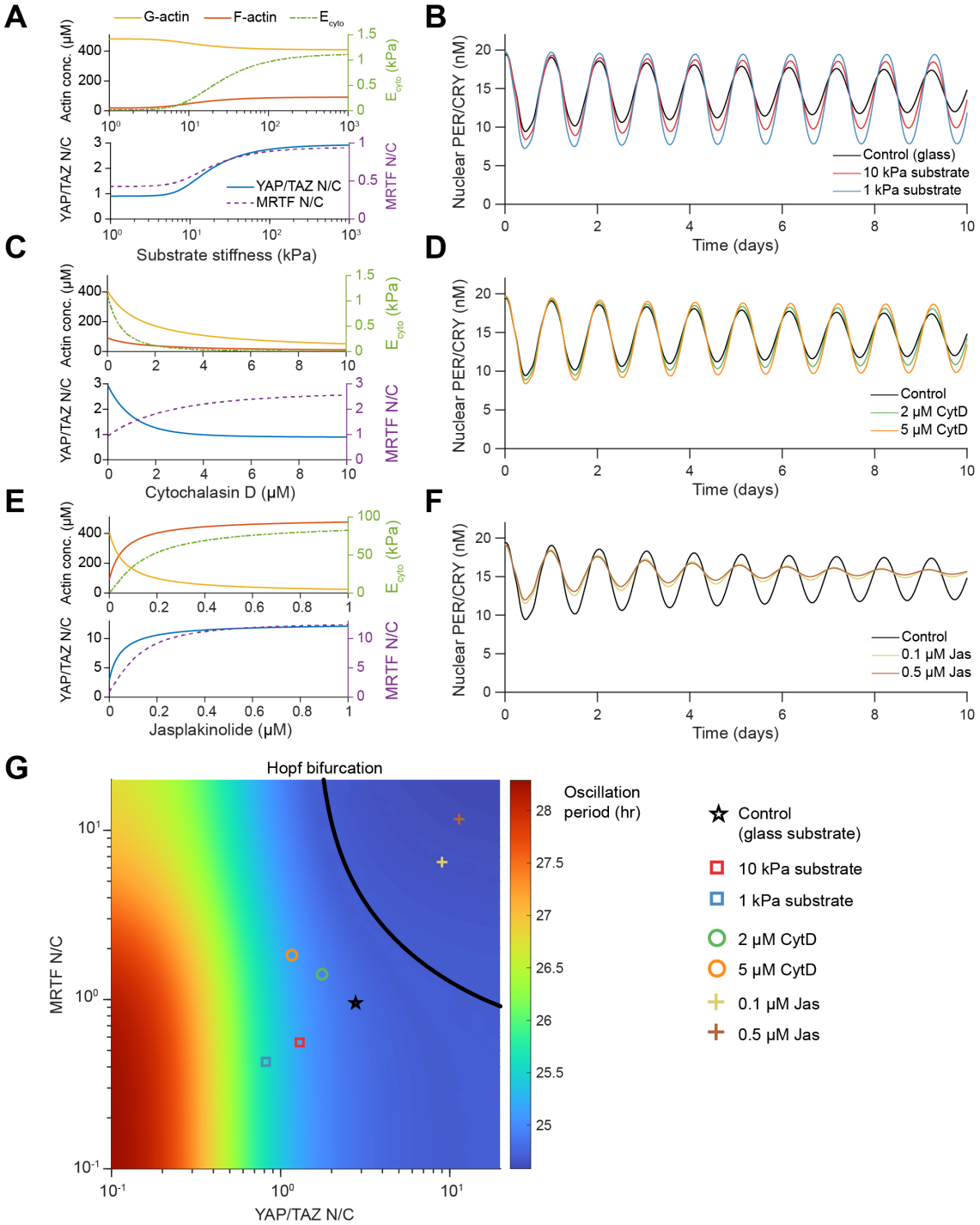

Figure 3: Changes to circadian oscillations due to altered cytoskeletal activity. (cont. on next page)

Figure 3: (cont. from previous page.) A) Substrate-stiffness-dependent changes in actin, cytosolic stiffness (E_{cyto}), nuclear YAP/TAZ, and nuclear MRTF. Cytoskeletal activity consistently increases with substrate stiffness, leading to elevated YAP/TAZ and MRTF nuclear to cytosolic ratios (N/C). B) Substrate-stiffness-dependent changes to oscillations in nuclear PER/CRY. On softer substrates, the circadian oscillation period is prolonged and PER2 amplitude is enhanced. C) Cytochalasin-D-induced changes to actin, cytosolic stiffness, and nuclear levels of YAP/TAZ and MRTF. Both F-actin and G-actin decrease with cytochalasin treatment, due to F-actin capping and G-actin dimerization. As a result, YAP/TAZ N/C decreases while MRTF N/C increases. D) Cytochalasin-D-induced changes to oscillations in nuclear PER/CRY. For lower amounts of actin polymerization, the circadian oscillation period is extended and PER2 amplitude is enhanced. E) Jasplakinolide-induced changes to actin, cytosolic stiffness, and nuclear levels of YAP/TAZ and MRTF. F-actin increases dramatically upon jasplakinolide treatment, leading to substantial nuclear accumulation of YAP/TAZ and MRTF. F) Jasplakinolide-induced changes to oscillations in nuclear PER/CRY. Increased actin polymerization leads to a slight decrease in the oscillation period along with a decay in circadian oscillations. G) Bifurcation diagram showing the location of the Hopf bifurcation and the dependence of the circadian oscillation period on nuclear YAP/TAZ and MRTF. All points to the left of the Hopf bifurcation curve correspond to sustained oscillations, whereas points to the right exhibit decaying oscillations. Individual markers plotted in the YAP/TAZ-MRTF phase plane correspond to the test cases shown in A-F.

soidal circadian oscillations). This metric corresponds to the fraction of the circadian power spectrum contained within a close window of the population-level average frequency, as detailed in Methods (Section "Calculation of the circadian power fraction"). Lower substrate stiffness are generally associated with higher circadian power fraction, whereas increased accumulation of YAP/TAZ and MRTF in the nucleus on stiff substrates results in lower circadian power fractions (Figure 4D). These lower circadian power fractions indicate significantly disrupted oscillations, which manifest as weaker oscillations that are drowned out by Gaussian noise in our simulations (Figure 4B). We note that Abenza *et al.* [15] did not observe the large increase in circadian power fraction on softer substrates that we report here; however, the average YAP/TAZ nuclear to cytosolic ratio also appears to remain elevated for cells on soft substrates in their study, perhaps indicating their cells remained in a mechanically active state not accounted for in our model.

Nuclear abundance of YAP/TAZ and MRTF correlate with the strength of circadian oscillations across treatment conditions

Next, we considered how other changes in the mechanical environment or distinct pharmacological treatments that disrupt the cytoskeleton can impact the the circadian power fraction. We tested the set of conditions examined experimentally in [15], including changes in substrate stiffness, cell density, or cell adhesion area, or treatment with cytochalasin D, latrunculin A, or blebbistatin. The assumed effects of each treatment are given in Table S3, with further details in the text of Supporting Information (Section S2). In brief, increased cell density and restriction of cell adhesion area (1600 or 900 μm^2 micropatterns) were both assumed to reduce the amount of FAK phosphorylation due

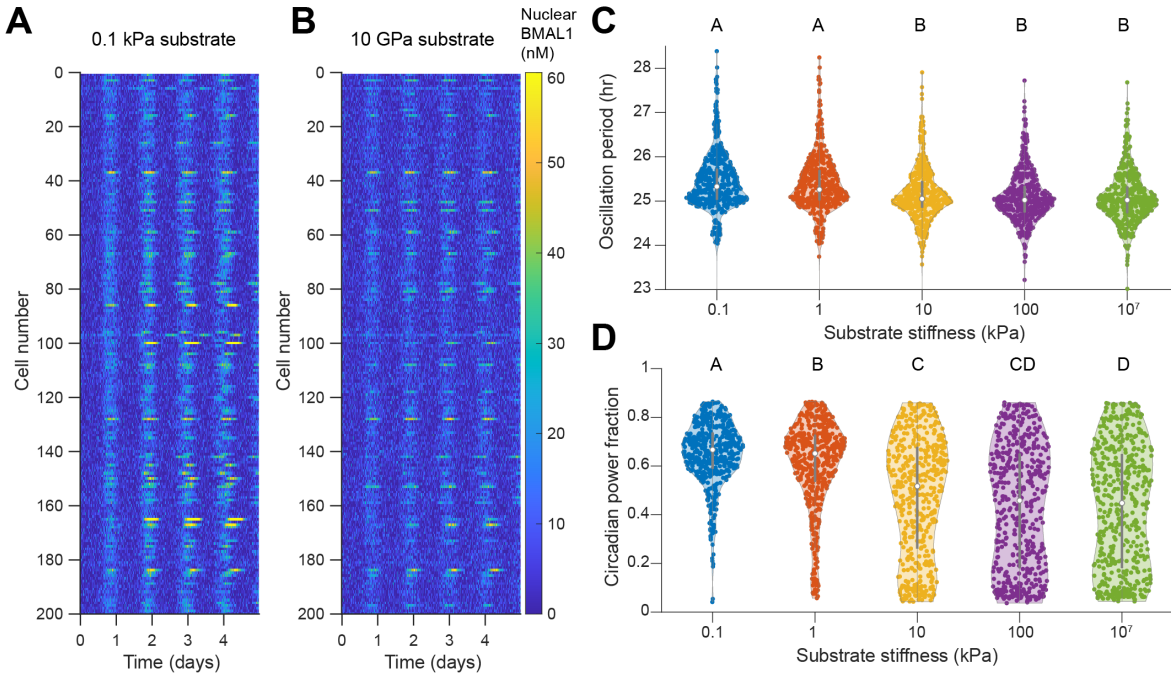

Figure 4: Behavior of circadian oscillations in model cell populations with variability. A) Kymograph depicting oscillations in nuclear BMAL1 for 200 model cells on a soft (0.1 kPa) substrate. Cells exhibit consistent circadian oscillations, while variability is observed at the level of the population. B) Kymograph depicting oscillations in nuclear BMAL1 for 200 model cells on glass (10 GPa). Most cells show consistent, lower magnitude oscillations; in some cases, oscillations are weaker or nonexistent. C-D) Distribution of oscillation period (C) and circadian power fraction (D) for cell populations on different substrate stiffnesses. Central points and error bars in violin plots denote the median and interquartile range. Compact letter display is used to denote statistical significance, where groups sharing a letter are statistically similar according to ANOVA followed by Tukey's *post hoc* test with a significance threshold of $p = 0.05$. Violin plots were generated using Violinplot in MATLAB [42]

to less cell-substrate contact (Section S2.4). Increased cell density was also assumed to increase the YAP/TAZ phosphorylation rate due to activation of LATS (Table S3). Latrunculin A and blebbistatin treatment decreased the F-actin polymerization rate and the formation of active stress fibers, respectively (Section S2.2, Table S3).

As expected, all of these treatments decrease nuclear YAP/TAZ and MRTF, with the exception of cytochalasin D, which increases the nuclear concentration of MRTF as described above (Figure 5). Given our previous results, we expect any treatments decreasing nuclear YAP/TAZ and/or MRTF to enhance circadian oscillations. Indeed, in all cases except cytochalasin D treatment, we do observe an increase in the median circadian power fraction (Figure 5).

In [15], the authors measured a significant correlation between YAP/TAZ nuclear to cytosolic ratio (N/C) and the circadian power fraction, but no such correlation for MRTF N/C. In agreement with their findings, we see a strong correlation between the power fraction and nuclear YAP/TAZ (Figure 5A). However, we also see a significant correlation of the power fraction with nuclear MRTF (Figure 5B). Notably, this correlation is weaker than that with YAP/TAZ (see correlation coefficient statistics in Figure 5). This agrees with our findings in Figure S4, where the stability of oscillations often depends most strongly on the amount of nuclear YAP/TAZ. Additionally, if we assume that substrate stiffness only moderately affects the circadian power fraction (as observed in [15]), the correlation with MRTF nuclear abundance is no longer significant, whereas the correlation with nuclear YAP/TAZ remains significant (Figure S5).

Computational predictions establish that YAP or LMNA mutations can significantly disrupt circadian oscillations

Both our single-cell model and our population-level models predict that YAP/TAZ and MRTF nuclear concentrations modulate the strength and stability of circadian oscillations (Figure 3G, Figure 4, Figure 5). We therefore reasoned that mutations affecting the associated pathways for nucleo-cytoplasmic transport could strongly impact circadian oscillations. We first tested this by considering the overexpression of the YAP mutant 5SA-YAP; such overexpression in fibroblasts was previously found to result in a large reduction in the circadian power fraction [15]. This mutant has several phosphorylation sites removed, causing it to accumulate at abnormal levels in the nucleus. We tested this condition in our model by introducing an equal amount of mutant 5SA-YAP as native YAP/TAZ and setting the phosphorylation rate of the 5SA-YAP to zero (Table S3). Due to the combined effects of overexpression and decreased phosphorylation, YAP/TAZ nuclear concentration significantly increases compared to wild type cells (Figure 6A). Separately, we tested possible effects of mutations in LMNA, the gene controlling the expression of lamin A. We consider a combination of two alterations

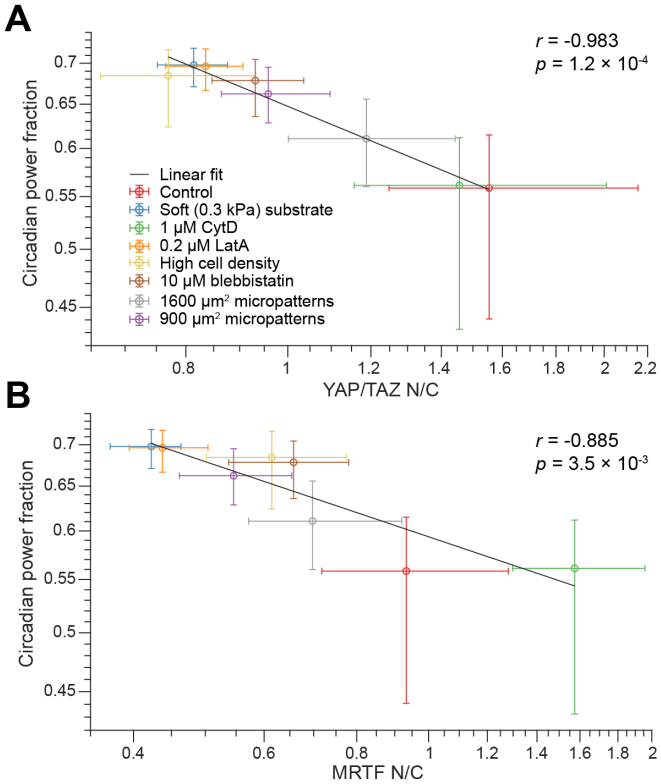

Figure 5: Correlation between circadian power fraction and nuclear to cytosolic ratios (N/C) of YAP/TAZ or MRTF. Populations of cells were subjected to the treatments from [15] and circadian power fraction was plotted against YAP/TAZ N/C (A) and MRTF N/C (B). Data points denote median values and error bars denote the range from the 40th to the 60th percentile for 500 model cells. In each case, Pearson's correlation coefficient (r) was assessed for the correlation between median power fraction and median N/C on the log scale. r and the p-value associated with the null hypothesis, $r = 0$, are included on each graph. To generate distinguishable colors for each condition, we used the linspecer tool in MATLAB [43].

to the model due to this mutation, aiming to mimic states relevant to laminopathies. Given that laminopathy-associated lamin mutants show distinct differences in their phosphorylation states [23, 44–46], we first assumed that mutated the lamin A was constitutively active (dephosphorylated). We additionally assumed that mutations in lamin A could result in increased nuclear permeability due to changes in localization of nuclear pore complexes (NPCs) or in overall nuclear shape (see, for instance, [47]). We set the lamin A phosphorylation rate to zero and doubled the opening rate of NPCs (Table S3), leading to increased levels of both YAP/TAZ and MRTF in the nucleus (Figure 6A-B), in agreement with recent experimental data [48].

On 30 kPa substrates, both mutants show altered BMAL1 dynamics, with significantly weaker oscillations compared to wild type cells (Figure 6C). The circadian power fraction decreases distinctly in each case, with the effect being relatively stronger for 5SA-YAP cells (Figure 6D). This is expected, given the dramatic increase in nuclear YAP/TAZ due to overexpression of 5SA-YAP, compared to the milder increases in both YAP/TAZ and MRTF observed for the lamin mutant (Figure 6A-B). This strong influence of 5SA-YAP overexpression on circadian power fraction agrees well with the findings in [15]. Our previous population-level tests establish that lower amounts of mechanical activation (e.g., lower substrate stiffness, treatment with cytoskeletal inhibitors) generally leads to increases in the circadian power fraction (Figure 4, Figure 5). Accordingly, we tested whether a reduction in substrate stiffness might rescue circadian oscillations for either mutant. Remarkably, we find that decreasing substrate stiffness to 3 kPa for the lamin A mutant, or to 0.3 kPa for the 5SA-YAP mutant, results in a power fraction statistically similar to wild type cells on 30 kPa (Figure 6E). This provides a prediction that can readily be tested experimentally. Furthermore, this may indicate a possible compensatory mechanism to counteract perturbations to circadian oscillations in laminopathies.

Discussion

24-hour cycles known as circadian rhythms are exhibited by most organisms on earth. Such oscillations can be observed in patterns of gene expression in single cells or in changes in organism-wide features such as body temperature. These changes in turn regulate physiological processes such as sleep-wake cycles and metabolic activity in healthy organisms. However, disruptions of regular circadian oscillations are associated with various diseases from cancer [6] to diabetes [7], placing a high priority on research efforts to understand the regulation of circadian rhythms from the cell to the organism level.

Several recent studies have found that local environmental cues such as substrate stiffness and cytoskeletal activity can modulate the cell circadian clock [12–15]. However, previous models of circadian

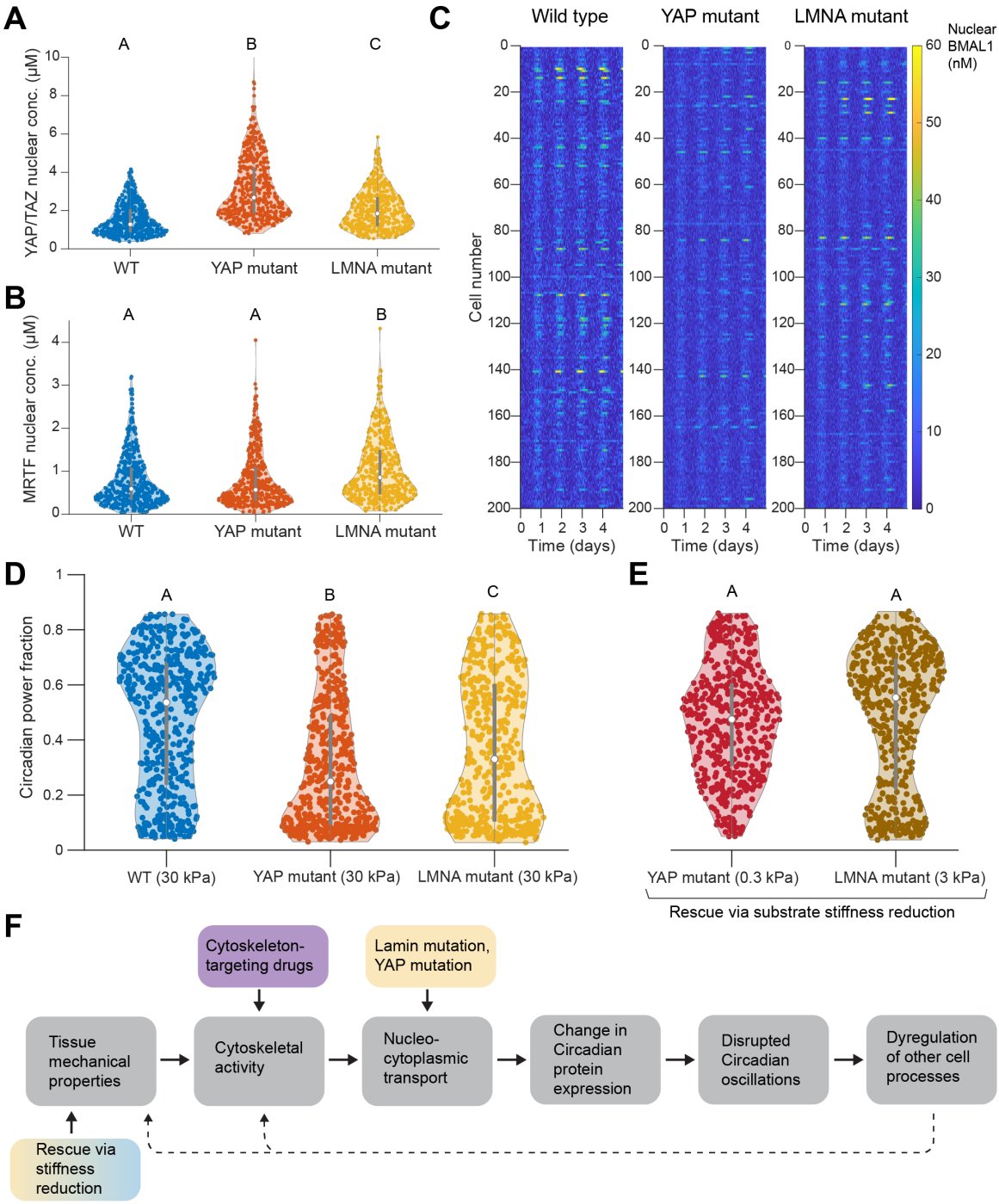

Figure 6: Effects of YAP or lamin A mutations on circadian oscillations. (cont. on next page)

Figure 6: (cont. from previous page.) A-B) Nuclear concentrations of YAP/TAZ (A) and MRTF (B) compared across wild type and both mutant populations on 30 kPa substrate. Overexpression of 5SA-YAP results in increased nuclear YAP/TAZ but not MRTF, whereas a mutation in LMNA causes elevations in both nuclear YAP/TAZ and MRTF. C) Kymograph depicting the dynamics of nuclear BMAL1 for a wild type population, YAP mutant population, and lamin A mutant population, all on 30 kPa substrates. Each plot shows 200 cells over 5 days; oscillations are visibly weaker for either mutation. D) Circadian power fraction compared across wild type and mutant cells on 30 kPa substrates. Mutations in YAP or LMNA each cause significant reductions in the power fraction. E) Rescue of normal circadian oscillations in mutant cells via reduction of substrate stiffness. The circadian power fraction for YAP mutant cells on a 0.3 kPa substrate, or LMNA mutant cells on a 3 kPa substrate, are statistically similar to that of wild type cells on a stiff (30 kPa) substrate. Central points and error bars in violin plots denote the median and interquartile range for populations of 500 cells each. Compact letter display is used to denote statistical significance, where groups sharing a letter are statistically similar according to ANOVA followed by Tukey's *post hoc* test with a significance threshold of $p = 0.05$. Violin plots were generated using Violinplot in MATLAB [42]. F) Summary of the causal flow from cell mechanotransduction to changes in the circadian clock. Upper colored boxes denote disruptions to mechanotransduction explored at different points in this paper, either due to cytoskeleton-targeting drugs or mutations in YAP or LMNA. The lower box depicts the rescue of normal circadian oscillations in mutant cells via a reduction in substrate stiffness. Dashed arrows indicate possible feedback from the circadian clock to cell and tissue mechanics.

oscillations in single cells do not include any effects on the expression of circadian proteins due to such factors. In our minimal model, we propose that nuclear YAP/TAZ and MRTF can alter the expression of BMAL1 and PER/CRY independently of other components of the circadian clock. As supported by recent experimental work [14, 15], this change in expression seems to be mediated by a combination of TEAD (in the case of YAP/TAZ) and SRF (in the case of MRTF). Although many of the mechanistic details behind this mechano-circadian coupling remain unclear, our calibrated model fits well to the experimental data and agrees with experimental measurements of cell populations. This suggests that YAP/TAZ and MRTF integrate different mechanical effects on cells, including actin polymerization, cytosolic stiffness, and myosin activity, to provide specific regulatory cues to the circadian clock.

From the main experimental work we draw from here [14, 15], the individual roles of YAP/TAZ and MRTF-mediated mechanotransduction remain unclear. While [14] focuses exclusively on MRTF-mediated activation of SRF, leading to changes in the expression of circadian proteins, [15] suggests that YAP/TAZ mediates changes in both BMAL1 and PER/CRY expression. In fact, it was shown in [15] that YAP/TAZ nuclear levels correlate with the circadian power fraction whereas MRTF nuclear levels do not. Results from our simulations indicate that these findings need not be contradictory. Although we assume that both YAP/TAZ and MRTF both mediate disruptions to the circadian clock, we find that YAP/TAZ correlates more strongly with the circadian power fraction (Figure 5). However, unlike in [15], we do observe a significant correlation between MRTF nuclear to cytosolic

ratio and circadian power fraction. This difference appears to come down to the assumed effect of substrate stiffness on the circadian power fraction; our model predicts a larger increase in power fraction for cells on soft substrates than that observed in [15]. Indeed, if we assume only a moderate increase in power fraction on softer substrates, the correlation with MRTF nuclear abundance is no longer significant, whereas the correlation with nuclear YAP/TAZ remains significant (Figure S5).

Our model predicts that certain mutations in YAP/TAZ or lamin A could significantly disrupt circadian oscillations in cell populations (Figure 6). In these cases, increased nuclear accumulation of YAP/TAZ and/or MRTF lead to perturbations to the circadian network such that oscillations are much weaker. This agrees well with experimental measurements in which overexpression or knockout of lamin A leads to significant changes in the expression of some circadian proteins [49]. Furthermore, these findings have natural implications for laminopathies, diseases that are characterized by mutations in LMNA. We specifically considered effects of LMNA mutations matching those previously found for laminopathy-associated mutations, including defects in lamin phosphorylation [44] and changes in NPC localization and nuclear shape [47]. Therefore, disruptions to the cell circadian clock could be one underappreciated component of disease state in laminopathies, as also posited in other recent work [49, 50]. For instance, due to the well-known role of the circadian clock in regulating metabolic processes [51], any such disruptions to the circadian clock could contribute to altered metabolism commonly observed in laminopathy patients [52, 53].

Our model may provide insights into other disease states as well. For instance, tissue stiffening is a common hallmark of diseases from cancer to atherosclerosis [17, 54]. As predicted by our model (Figure 4), increased substrate stiffness could locally perturb circadian oscillations in cells. Given the host of cellular processes regulated by circadian cues, any such disruptions could have large effects on overall cell function. Additionally, the results of our *in silico* rescue experiment (Figure 6F) suggest that changes in the local mechanical properties of tissue could serve to counteract disruptions to normal circadian oscillations in diseased cells. For instance, a 10-fold reduction (from 30 kPa to 3 kPa) is sufficient to rescue normal circadian oscillations in our simulated LMNA mutant. This may provide an inherent biological strategy to recover normal oscillations in diseases such as laminopathies. Overall, these findings suggest that mutations affecting nuclear transport render cells especially vulnerable to dysfunctions in circadian oscillations upon tissue stiffening.

Other factors currently not considered in our model could have important effects on the nuclear translocation of YAP/TAZ and MRTF, thereby influencing any downstream disruptions to circadian oscillations. For instance, the disruptive effect of substrate stiffness on circadian oscillations could be slightly alleviated for cells in 3D culture conditions, as previous modeling work shows that cells

simulated in 2D culture have higher YAP/TAZ N/C compared to cells in 3D culture [22]. Moreover, changes in cell shape are known to influence YAP/TAZ nuclear translocation [22, 55]. Finally, many other pathways such as calcium signaling cascades are known to play important roles in determining the YAP/TAZ N/C [56]. These various factors provide natural areas for future extensions of our model.

As it stands, the coupling in our model goes only one way; that is, YAP/TAZ and MRTF alter the expression of circadian proteins. In reality, changes to the circadian oscillation period may induce other changes in cell physiology which could couple back to the mechanical state of cells and/or tissue, creating a closed feedback loop (Figure 6F). For instance, the circadian clock plays an important regulatory role in ECM remodeling, controlling processes from collagen deposition to MMP activity [57, 58]. Rather than assuming the cell reaches mechanical steady state prior to the start of the simulation, YAP/TAZ and MRTF dynamics could readily be integrated within our equations. In the future, this approach would give us a unique opportunity to probe the complex interplay between circadian clocks, mechanotransduction, and disease states.

Methods

Numerical implementation

Our code is implemented in MATLAB 2023, and is freely available at https://github.com/RangamaniLabUCSD/MechanoCircadian. Given the set of treatment conditions (substrate stiffness, cell density, inhibitor concentrations), we algebraically solved for the steady-state concentrations of nuclear YAP/TAZ and nuclear MRTF. These values were then used to compute K_{eB2} and K_{eP2} (Equations (3) and (4)), and the resulting system of DDEs (Equations (5) and (6)) was solved using dde23. As initial conditions in dde23, we used $B_0 = 5B^*$ and $P_0 = 0.2P^*$, where B^* and P^* were the steady-state BMAL1 and PER/CRY values associated with a given treatment condition. The luceriferase concentration, $L(t)$, was then computed by integrating Equation (7) using ode15s, with the initial condition $L_0 = 0$.

Sensitivity analysis and parameter estimation

We conducted a global parametric sensitivity analysis using the UQLab framework in MATLAB [59]. Treating the luciferase oscillation period and amplitude as quantities of interest, we estimated the total-order Sobol indices associated with parameters from Table 2 and Table 1. These represent the total effect of a parameter on the given output, including first-order effects and all higher-order effects arising from interactions with other parameters We only considered the case of untreated cells on glass

(10 GPa stiffness) and did not test the sensitivity to any inhibitor-related parameters.

We completed our model calibration using Bayesian parameter estimation in UQLab, allowing us estimate likelihood distributions for each parameter given the mean experimental measurements and associated errors. As a log likelihood function, we used the negative weighted sum of square errors between the experimental dynamics and predicted luciferase dynamics across all conditions (Equation (S32)). We solved for the posterior distributions using Markov chain Monte Carlo (MCMC) in UQLab, with 60 chains extended out to 10,000 steps total. Additional details on this fitting procedure are provided in Supporting Information (Section S3), and the posterior distributions for each parameter are plotted in Figure S1.

Linear stability analysis

To assess which parameters naturally give rise to sustained circadian oscillations, we conducted a linear stability analysis. We initially approached this analytically, which allowed us examine the stability of a simplified version of the system in which the equations for B and P are decoupled ($K_{dBP} = 0$) (Section S4). To probe the stability of the entire system with no simplifications, we conducted numerical bifurcation analysis using DDE-BIFTOOL in MATLAB [60]. For this analysis, we used the maximum *a posteriori* (MAP) values as point estimates for each circadian parameter (Table 2) and treated the nuclear to cytosolic ratios of YAP/TAZ and MRTF as bifurcation parameters. In this context, the Hopf bifurcation is defined by the transition of the rightmost (most positive / least negative) pair of eigenvalues from negative real values to positive real values (Figure S4B). This corresponds to a supercritical Hopf bifurcation, in which damped oscillations transition to a stable limit cycle.

Given the known importance of degradation rates on circadian oscillations, we also examined the effects of K_{dB}, K_{dP}, and K_{dBP} on the location of Hopf bifurcations and the period of oscillations (Figure S4). These results are further discussed in Section S4.

Simulation of cell populations

We generated model populations of cells by sampling parameter values from probability distributions. By default, we sample all parameters in our YAP/TAZ mechanotransduction model from log-normal distributions. We selected parameter values from each distribution by first generating a normally distributed random number r using randn() in MATLAB, and then computing:

$$k = \bar{k}e^{\sigma_k r}, \tag{8}$$

where σ_k is the standard deviation associated with the log-normal distribution of values for k and $\bar{k}$ is the baseline value of the parameter. A value of $\sigma = 0.2$ was used for all parameters except any exponents, which were kept constant.

For all MRTF and circadian parameters fit using the Bayesian approach described above, their probability distributions were described by their posterior distributions (Figure S1). We randomly drew from these distributions by sampling from the MCMC chains after discarding the first 5,000 iterations as burn-in.

Calculation of the circadian power fraction

We used the circadian power fraction as a metric for the quality of circadian oscillations, as defined by Abenza *et al.* [15]. In their paper, they measured circadian oscillations using the fluorescent sensor REV-VNP [61] as an indicator for REV-ERBα expression. Because our model does not explicitly include REV-ERBα, we instead computed the power fraction of BMAL1, which directly positively regulates the expression of REV-ERBα [3]. Before computing the power fraction, we added white Gaussian noise to individual BMAL1 trajectories, assuming a signal-to-noise ratio of 5. We sampled the resulting signal every 15 minutes (sampling frequency $f_S = 96$ day^{-1}) and then filtered it using a low pass filter with the same settings as in Abenza *et al.* (filtfilt() in MATLAB with a = 1 and b = (0.2, 0.2, 0.2, 0.2)) and scaled the dynamics by subtracting the mean and dividing by the standard deviation. We then computed the power spectrum, $\mathcal{P}$, for each cell in the model population for a given condition. The power fraction for an individual cell was then given by:

$$\mathcal{P}_{frac} = \frac{\int_{f_C-0.2}^{f_C+0.2} \mathcal{P} df}{\int_0^{2f_S} \mathcal{P} df}, \tag{9}$$

where f_C is the frequency associated with the maximum population-wide average power in the interval 0.7 day^{-1} to 1.3 day^{-1}.

Acknowledgements

This work was supported in part by the Wu Tsai Human Performance Alliance at UCSD to P.R. E.A.F. is supported by the National Science Foundation under Grant # EEC-2127509 to the American Society for Engineering Education.

Supporting Figures

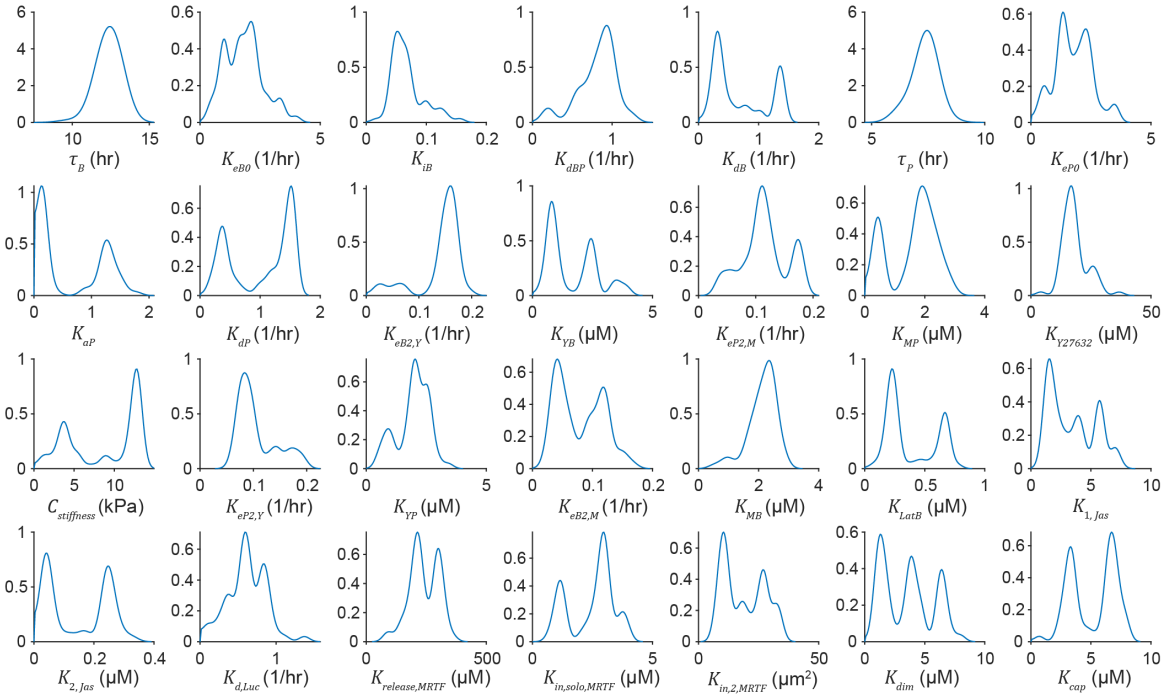

Figure S1: Parameter posterior distributions from Bayesian parameter estimation. Markov chain Monte Carlo (MCMC) was run for 10,000 iterations with 60 walkers. After discarding the first 5,000 iterations as burn-in, posterior distributions were estimated using kernel density estimation in MATLAB, with a bandwidth of 5% of the maximum value of a given parameter included in the prior distribution.

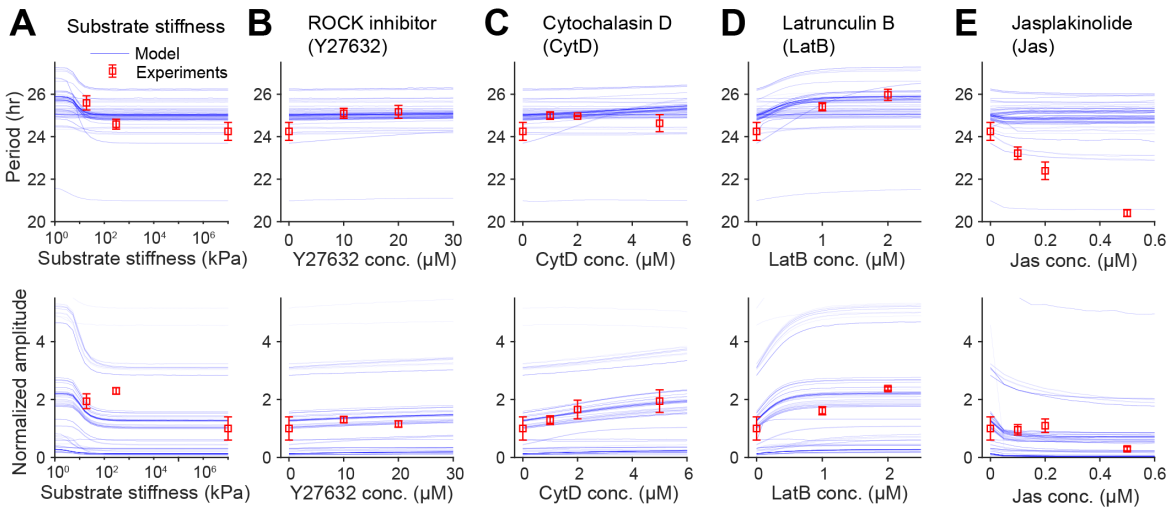

Figure S2: Circadian period and amplitude for different samples from the posterior distribution. Period and amplitude are plotted for different treatment conditions, for 250 different samples each.

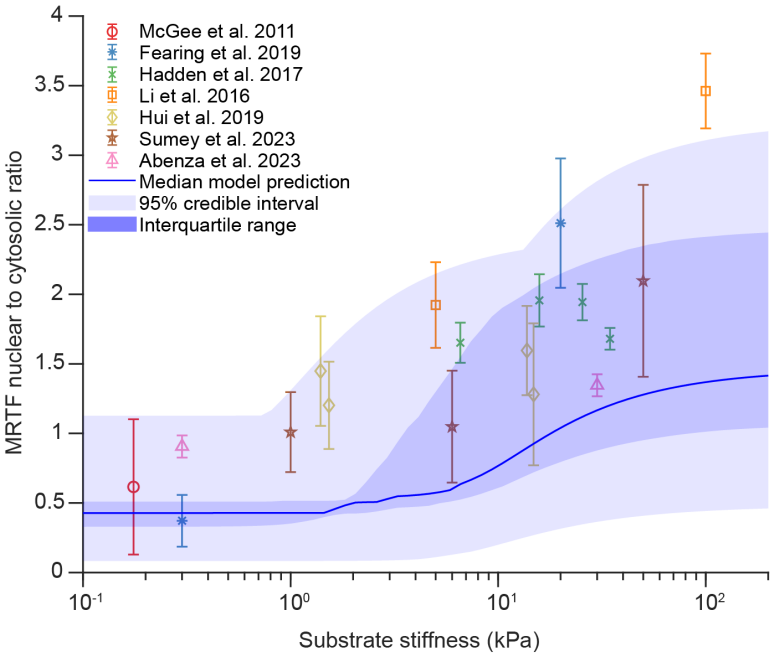

Figure S3: Model predictions for MRTF nuclear to cytosolic ratio vs. substrate stiffness. Experimental data (mean ± standard deviation) is plotted for MRTF nuclear to cytosolic ratios in 7 different studies [15, 62–67]. Solid blue line shows the median model prediction at each substrate stiffness, the darker blue region indicates interquartile range, and the lighter blue region spans the 95% credible interval (region from the 2.5 percentile to 97.5 percentile).

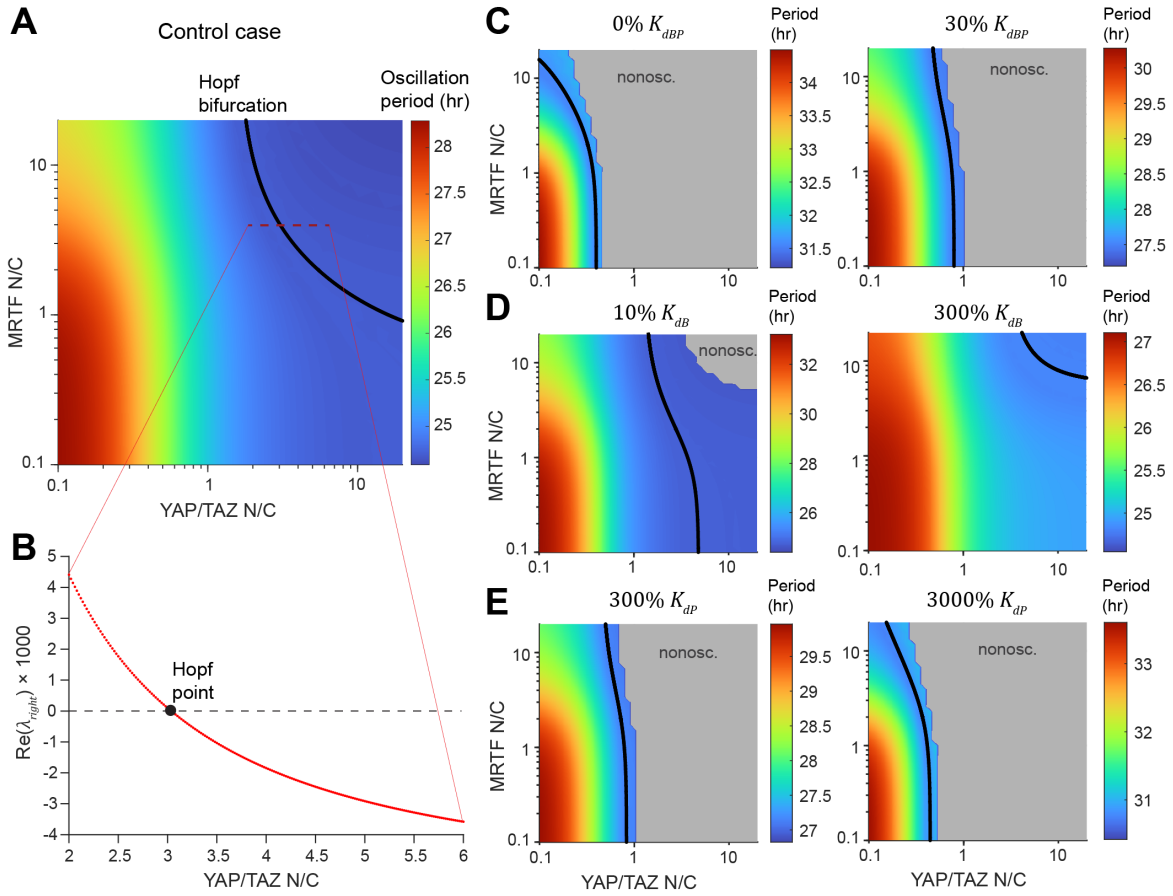

Figure S4: Stability analysis for different parameter values. A) Control bifurcation diagram, with oscillation period and location of the Hopf bifurcation plotted as a function of YAP/TAZ and MRTF nuclear to cytosolic ratios (N/C). B) The real part of the right-most pair of eigenvalues (λ_{right}) along the line where MRTF N/C is 4 (red dashed line in panel A). The transition from positive to negative real part of the eigenvalues marks the occurrence of a Hopf bifurcation as shown. After identification of the bifurcation in this manner, we can continue along the Hopf bifurcation using DDE-BIFTOOL to generate the full bifurcation curve. C) Effects of decreasing K_{dBP} (0% or 30% of the maximum *a posteriori* value) on the location of the Hopf bifurcation and the oscillation period. The grey region denotes nonoscillatory solutions. Smaller K_{dBP} values are associated with a smaller region of phase space exhibiting oscillatory solutions. D) Effects of decreasing or increasing K_{dB} (10% or 300% of the maximum *a posteriori* value) on the location of the Hopf bifurcation and the oscillation period. Similar to above, smaller K_{dB} values are associated with a smaller region of phase space exhibiting oscillatory solutions. E) Effects of increasing K_{dP} (300% or 3000% of the maximum *a posteriori* value) on the location of the Hopf bifurcation and the oscillation period. In this case, larger K_{dP} values are associated with a smaller region of phase space exhibiting oscillatory solutions.

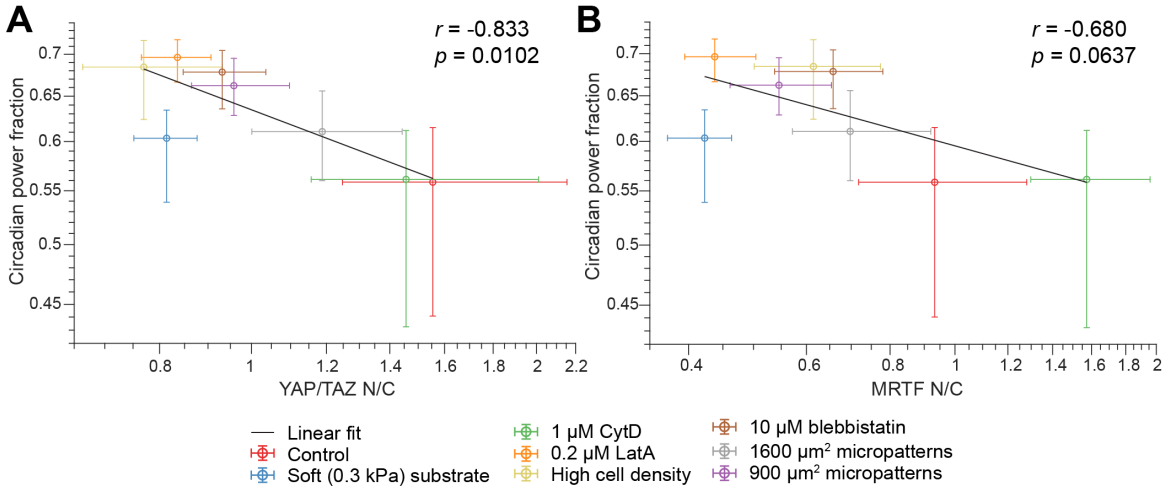

Figure S5: Altered power fraction / transcriptional regulator correlation with reduced circadian sensitivity to stiffness. Reducing the circadian power fraction for cells on a soft substrate changes the correlations between circadian power fraction and YAP/TAZ N/C (A) or the MRTF N/C (B). In this case, we altered the power fraction for cells on a soft substrate by averaging that of cells on a soft substrate and cells on a stiff substrate. Pearson's correlation coefficient (between median YAP/TAZ or MRTF N/C and median circadian power fraction, both on the log scale), r, and the p-value associated with the null hypothesis, $r = 0$, are included on each graph. Data points denote median and error bars denote the range from the 40th to the 60th percentile for 500 model cells. To generate distinguishable colors for each condition, we used the linspecer tool in MATLAB [43].

References

[1] David K. Welsh, Joseph S. Takahashi, and Steve A. Kay. "Suprachiasmatic Nucleus: Cell Autonomy and Network Properties". In: *Annual Review of Physiology* 72.1 (Mar. 17, 2010), pp. 551–577. ISSN: 0066-4278, 1545-1585.

[2] Jennifer A Evans. "Collective Timekeeping among Cells of the Master Circadian Clock". In: *Journal of Endocrinology* 230.1 (July 2016), R27–R49. ISSN: 0022-0795, 1479-6805.

[3] Joseph S. Takahashi. "Transcriptional Architecture of the Mammalian Circadian Clock". In: *Nature Reviews Genetics* 18.3 (Mar. 2017), pp. 164–179. ISSN: 1471-0056, 1471-0064.

[4] Ethan D. Buhr and Joseph S. Takahashi. "Molecular Components of the Mammalian Circadian Clock". In: *Circadian Clocks*. Ed. by Achim Kramer and Martha Merrow. Vol. 217. Berlin, Heidelberg: Springer Berlin Heidelberg, 2013, pp. 3–27. ISBN: 978-3-642-25949-4 978-3-642-25950-0.

[5] Ray Zhang, Nicholas F. Lahens, Heather I. Ballance, Michael E. Hughes, and John B. Hogenesch. "A Circadian Gene Expression Atlas in Mammals: Implications for Biology and Medicine". In: *Proceedings of the National Academy of Sciences* 111.45 (Nov. 11, 2014), pp. 16219–16224. ISSN: 0027-8424, 1091-6490.

[6] Ayesha A. Shafi and Karen E. Knudsen. "Cancer and the Circadian Clock". In: *Cancer Research* 79.15 (Aug. 1, 2019), pp. 3806–3814. ISSN: 0008-5472, 1538-7445.

[7] Ivy C. Mason, Jingyi Qian, Gail K. Adler, and Frank A. J. L. Scheer. "Impact of Circadian Disruption on Glucose Metabolism: Implications for Type 2 Diabetes". In: *Diabetologia* 63.3 (Mar. 2020), pp. 462–472. ISSN: 0012-186X, 1432-0428.

[8] Charles H. Streuli and Qing-Jun Meng. "Influence of the Extracellular Matrix on Cell-Intrinsic Circadian Clocks". In: *Journal of Cell Science* 132.3 (Feb. 1, 2019), jcs207498. ISSN: 1477-9137, 0021-9533.

[9] Aurélio Balsalobre, Francesca Damiola, and Ueli Schibler. "A Serum Shock Induces Circadian Gene Expression in Mammalian Tissue Culture Cells". In: *Cell* 93.6 (June 1998), pp. 929–937. ISSN: 00928674.

[10] Alan Gerber et al. "Blood-Borne Circadian Signal Stimulates Daily Oscillations in Actin Dynamics and SRF Activity". In: *Cell* 152.3 (Jan. 2013), pp. 492–503. ISSN: 00928674.

[11] Cyril Esnault et al. "Rho-Actin Signaling to the MRTF Coactivators Dominates the Immediate Transcriptional Response to Serum in Fibroblasts". In: *Genes & Development* 28.9 (May 1, 2014), pp. 943–958. ISSN: 0890-9369, 1549-5477.

[12] Nan Yang et al. "Cellular Mechano-Environment Regulates the Mammary Circadian Clock". In: *Nature Communications* 8.1 (Jan. 30, 2017), p. 14287. ISSN: 2041-1723.

[13] Jack Williams et al. "Epithelial and Stromal Circadian Clocks Are Inversely Regulated by Their Mechano-Matrix Environment". In: *Journal of Cell Science* (Jan. 1, 2018), jcs.208223. ISSN: 1477-9137, 0021-9533.

[14] Xuekai Xiong et al. "The Actin Cytoskeleton-MRTF/SRF Cascade Transduces Cellular Physical Niche Cues to Entrain the Circadian Clock". In: *Journal of Cell Science* 135.19 (Oct. 1, 2022), jcs260094. ISSN: 0021-9533, 1477-9137.

[15] Juan F. Abenza et al. "Mechanical Control of the Mammalian Circadian Clock via YAP/TAZ and TEAD". In: *Journal of Cell Biology* 222.9 (Sept. 4, 2023), e202209120. ISSN: 0021-9525, 1540-8140.

[16] Paul A. Janmey, Daniel A. Fletcher, and Cynthia A. Reinhart-King. "Stiffness Sensing by Cells". In: *Physiological Reviews* 100.2 (Apr. 1, 2020), pp. 695–724. ISSN: 0031-9333, 1522-1210.

[17] LiKang Chin, Yuntao Xia, Dennis E Discher, and Paul A Janmey. "Mechanotransduction in Cancer". In: *Current Opinion in Chemical Engineering* 11 (Feb. 2016), pp. 77–84. ISSN: 22113398.

[18] Ameneh Asgari-Targhi and Elizabeth B. Klerman. "Mathematical Modeling of Circadian Rhythms". In: *WIREs Systems Biology and Medicine* 11.2 (Mar. 2019). ISSN: 1939-5094, 1939-005X.

[19] Jean-Christophe Leloup and Albert Goldbeter. "Toward a Detailed Computational Model for the Mammalian Circadian Clock". In: *Proceedings of the National Academy of Sciences* 100.12 (June 10, 2003), pp. 7051–7056. ISSN: 0027-8424, 1091-6490.

[20] Martín A. Lema, Diego A. Golombek, and Julián Echave. "Delay Model of the Circadian Pacemaker". In: *Journal of Theoretical Biology* 204.4 (June 2000), pp. 565–573. ISSN: 00225193.

[21] Meng Sun, Fabian Spill, and Muhammad H. Zaman. "A Computational Model of YAP/TAZ Mechanosensing". In: *Biophysical Journal* 110.11 (June 2016), pp. 2540–2550. ISSN: 00063495.

[22] Kiersten Elizabeth Scott, Stephanie I. Fraley, and Padmini Rangamani. "A Spatial Model of YAP/TAZ Signaling Reveals How Stiffness, Dimensionality, and Shape Contribute to Emergent Outcomes". In: *Proceedings of the National Academy of Sciences* 118.20 (May 18, 2021), e2021571118. ISSN: 0027-8424, 1091-6490.

[23] Joe Swift et al. "Nuclear Lamin-A Scales with Tissue Stiffness and Enhances Matrix-Directed Differentiation". In: *Science* 341.6149 (Aug. 30, 2013), p. 1240104. ISSN: 0036-8075, 1095-9203.

[24] Michael R. Bubb, Ilan Spector, Bret B. Beyer, and Katina M. Fosen. "Effects of Jasplakinolide on the Kinetics of Actin Polymerization". In: *Journal of Biological Chemistry* 275.7 (Feb. 2000), pp. 5163–5170. ISSN: 00219258.

[25] K. Sriram, Gilles Bernot, and François Képès. "Discrete Delay Model for the Mammalian Circadian Clock". In: *Complexus* 3.4 (2006), pp. 185–199. ISSN: 1424-8492, 1424-8506.

[26] Paul Smolen, Douglas A. Baxter, and John H. Byrne. "Modeling Circadian Oscillations with Interlocking Positive and Negative Feedback Loops". In: *The Journal of Neuroscience* 21.17 (Sept. 1, 2001), pp. 6644–6656. ISSN: 0270-6474, 1529-2401.

[27] Lauren P. Shearman et al. "Interacting Molecular Loops in the Mammalian Circadian Clock". In: *Science* 288.5468 (May 12, 2000), pp. 1013–1019. ISSN: 0036-8075, 1095-9203.

[28] Teruya Tamaru et al. "Nucleocytoplasmic Shuttling and Phosphorylation of BMAL1 Are Regulated by Circadian Clock in Cultured Fibroblasts: Circadian BMAL1 Nucleocytoplasmic Shuttling". In: *Genes to Cells* 8.12 (Dec. 2003), pp. 973–983. ISSN: 13569597.

[29] Kazuhiro Yagita, Filippo Tamanini, Gijsbertus T. J. Van Der Horst, and Hitoshi Okamura. "Molecular Mechanisms of the Biological Clock in Cultured Fibroblasts". In: *Science* 292.5515 (Apr. 13, 2001), pp. 278–281. ISSN: 0036-8075, 1095-9203.

[30] Kazuhiro Yagita et al. "Nucleocytoplasmic Shuttling and mCRY-dependent Inhibition of Ubiquitylation of the mPER2 Clock Protein". In: *The EMBO Journal* 21.6 (Mar. 15, 2002), pp. 1301–1314. ISSN: 02614189.

[31] Choogon Lee, Jean-Pierre Etchegaray, Felino R.A. Cagampang, Andrew S.I. Loudon, and Steven M. Reppert. "Posttranslational Mechanisms Regulate the Mammalian Circadian Clock". In: *Cell* 107.7 (Dec. 2001), pp. 855–867. ISSN: 00928674.

[32] Seung-Hee Yoo et al. "PERIOD2::LUCIFERASE Real-Time Reporting of Circadian Dynamics Reveals Persistent Circadian Oscillations in Mouse Peripheral Tissues". In: *Proceedings of the National Academy of Sciences* 101.15 (Apr. 13, 2004), pp. 5339–5346. ISSN: 0027-8424, 1091-6490.

[33] Kevin A. Feeney, Marrit Putker, Marco Brancaccio, and John S. O'Neill. "In-Depth Characterization of Firefly Luciferase as a Reporter of Circadian Gene Expression in Mammalian Cells". In: *Journal of Biological Rhythms* 31.6 (Dec. 2016), pp. 540–550. ISSN: 0748-7304, 1552-4531.

[34] Nicola J. Smyllie et al. "Visualizing and Quantifying Intracellular Behavior and Abundance of the Core Circadian Clock Protein PERIOD2". In: *Current Biology* 26.14 (July 2016), pp. 1880–1886. ISSN: 09609822.

[35] Nathaniel J. Linden, Boris Kramer, and Padmini Rangamani. "Bayesian Parameter Estimation for Dynamical Models in Systems Biology". In: *PLOS Computational Biology* 18.10 (Oct. 21, 2022). Ed. by Jeffrey J. Saucerman, e1010651. ISSN: 1553-7358.

[36] T. Wakatsuki, B. Schwab, N.C. Thompson, and E.L. Elson. "Effects of Cytochalasin D and Latrunculin B on Mechanical Properties of Cells". In: *Journal of Cell Science* 114.5 (Mar. 1, 2001), pp. 1025–1036. ISSN: 1477-9137, 0021-9533.

[37] Megan Finch-Edmondson and Marius Sudol. "Framework to Function: Mechanosensitive Regulators of Gene Transcription". In: *Cellular & Molecular Biology Letters* 21.1 (Dec. 2016), p. 28. ISSN: 1425-8153, 1689-1392.

[38] Francesc Miralles, Guido Posern, Alexia-Ileana Zaromytidou, and Richard Treisman. "Actin Dynamics Control SRF Activity by Regulation of Its Coactivator MAL". In: *Cell* 113.3 (May 2003), pp. 329–342. ISSN: 00928674.

[39] Haibo Ni, Stefano Morotti, and Eleonora Grandi. "A Heart for Diversity: Simulating Variability in Cardiac Arrhythmia Research". In: *Frontiers in Physiology* 9 (July 20, 2018), p. 958. ISSN: 1664-042X.

[40] Divya C. Kernik et al. "A Computational Model of Induced Pluripotent Stem-cell Derived Cardiomyocytes Incorporating Experimental Variability from Multiple Data Sources". In: *The Journal of Physiology* 597.17 (Sept. 2019), pp. 4533–4564. ISSN: 0022-3751, 1469-7793.

[41] Alan Veliz-Cuba et al. "Sources of Variability in a Synthetic Gene Oscillator". In: *PLOS Computational Biology* 11.12 (Dec. 22, 2015). Ed. by Gabor Balazsi, e1004674. ISSN: 1553-7358.

[42] Bastian Bechtold. *Violin Plots for MATLAB*. 2016.

[43] Jonathan Lansey. *Beautiful and Distinguishable Line Colors + Colormap*. 2023.

[44] Elin Torvaldson, Vitaly Kochin, and John E Eriksson. "Phosphorylation of Lamins Determine Their Structural Properties and Signaling Functions". In: *Nucleus* 6.3 (May 4, 2015), pp. 166–171. ISSN: 1949-1034, 1949-1042.

[45] V Cenni. "Lamin A N-terminal Phosphorylation Is Associated with Myoblast Activation: Impairment in Emery-Dreifuss Muscular Dystrophy". In: *Journal of Medical Genetics* 42.3 (Mar. 1, 2005), pp. 214–220. ISSN: 1468-6244.

[46] Hiroaki Mitsuhashi et al. "Specific Phosphorylation of Ser458 of A-type Lamins in *LMNA* - Associated Myopathy Patients". In: *Journal of Cell Science* 123.22 (Nov. 15, 2010), pp. 3893–3900. ISSN: 1477-9137, 0021-9533.

[47] Subarna Dutta et al. "Skeletal Muscle Dystrophy Mutant of Lamin A Alters the Structure and Dynamics of the Ig Fold Domain". In: *Scientific Reports* 8.1 (Sept. 14, 2018), p. 13793. ISSN: 2045-2322.

[48] Daniel J. Owens et al. "Lamin Mutations Cause Increased YAP Nuclear Entry in Muscle Stem Cells". In: *Cells* 9.4 (Mar. 27, 2020), p. 816. ISSN: 2073-4409.

[49] Clare Amy Roskell. "The Role of Nuclear Lamins in Regulating the Circadian Molecular Clockwork; Daily Oscillations and Response to Mechanical Stimulation". PhD thesis. England: The University of Liverpool (United Kingdom), 2019. 317 pp. ISBN: 9798664774535.

[50] Nolwenn Briand and Philippe Collas. "Laminopathy-Causing Lamin A Mutations Reconfigure Lamina-Associated Domains and Local Spatial Chromatin Conformation". In: *Nucleus* 9.1 (Dec. 31, 2018), pp. 216–226. ISSN: 1949-1034, 1949-1042.

[51] Saurabh Sahar and Paolo Sassone-Corsi. "Regulation of Metabolism: The Circadian Clock Dictates the Time". In: *Trends in Endocrinology & Metabolism* 23.1 (Jan. 2012), pp. 1–8. ISSN: 10432760.

[52] Aurélie Decaudain et al. "New Metabolic Phenotypes in Laminopathies: *LMNA* Mutations in Patients with Severe Metabolic Syndrome". In: *The Journal of Clinical Endocrinology & Metabolism* 92.12 (Dec. 1, 2007), pp. 4835–4844. ISSN: 0021-972X, 1945-7197.

[53] A.C. Guénantin et al. "Nuclear Envelope-Related Lipodystrophies". In: *Seminars in Cell & Developmental Biology* 29 (May 2014), pp. 148–157. ISSN: 10849521.

[54] Carlo Palombo and Michaela Kozakova. "Arterial Stiffness, Atherosclerosis and Cardiovascular Risk: Pathophysiologic Mechanisms and Emerging Clinical Indications". In: *Vascular Pharmacology* 77 (Feb. 2016), pp. 1–7. ISSN: 15371891.

[55] Kerbaï Saïd Eroumé, Rachel Cavill, Katerina Staňková, Jan De Boer, and Aurélie Carlier. "Exploring the Influence of Cytosolic and Membrane FAK Activation on YAP/TAZ Nuclear Translocation". In: *Biophysical Journal* 120.20 (Oct. 2021), pp. 4360–4377. ISSN: 00063495.

[56] A. Khalilimeybodi, S.I. Fraley, and P. Rangamani. "Mechanisms Underlying Divergent Relationships between Ca^{2+} and YAP/TAZ Signalling". In: *The Journal of Physiology* 601.3 (Feb. 2023), pp. 483–515. ISSN: 0022-3751, 1469-7793.

[57] Michal Dudek, Joe Swift, and Qing-Jun Meng. "The Circadian Clock and Extracellular Matrix Homeostasis in Aging and Age-Related Diseases". In: *American Journal of Physiology-Cell Physiology* 325.1 (July 1, 2023), pp. C52–C59. ISSN: 0363-6143, 1522-1563.

[58] Kameron Hahn and Isaac Kirubakaran Sundar. "Current Perspective on the Role of the Circadian Clock and Extracellular Matrix in Chronic Lung Diseases". In: *International Journal of Environmental Research and Public Health* 20.3 (Jan. 30, 2023), p. 2455. ISSN: 1660-4601.

[59] Stefano Marelli and Bruno Sudret. "UQLab: A Framework for Uncertainty Quantification in Matlab". In: *Vulnerability, Uncertainty, and Risk*. Second International Conference on Vulnerability and Risk Analysis and Management (ICVRAM) and the Sixth International Symposium on Uncertainty, Modeling, and Analysis (ISUMA). Liverpool, UK: American Society of Civil Engineers, June 27, 2014, pp. 2554–2563. ISBN: 978-0-7844-1360-9.

[60] K. Engelborghs, T. Luzyanina, and D. Roose. "Numerical Bifurcation Analysis of Delay Differential Equations Using DDE-BIFTOOL". In: *ACM Transactions on Mathematical Software* 28.1 (Mar. 2002), pp. 1–21. ISSN: 0098-3500, 1557-7295.

[61] Emi Nagoshi et al. "Circadian Gene Expression in Individual Fibroblasts". In: *Cell* 119.5 (Nov. 2004), pp. 693–705. ISSN: 00928674.

[62] Karen M McGee, Maria K Vartiainen, Peng T Khaw, Richard Treisman, and Maryse Bailly. "Nuclear Transport of the Serum Response Factor Coactivator MRTF-A Is Downregulated at Tensional Homeostasis". In: *EMBO reports* 12.9 (Sept. 2011), pp. 963–970. ISSN: 1469-221X, 1469-3178.

[63] Bailey V. Fearing et al. "Mechanosensitive Transcriptional Coactivators MRTF-A and YAP/TAZ Regulate Nucleus Pulposus Cell Phenotype through Cell Shape". In: *The FASEB Journal* 33.12 (Dec. 2019), pp. 14022–14035. ISSN: 0892-6638, 1530-6860.

[64] William J. Hadden et al. "Stem Cell Migration and Mechanotransduction on Linear Stiffness Gradient Hydrogels". In: *Proceedings of the National Academy of Sciences* 114.22 (May 30, 2017), pp. 5647–5652. ISSN: 0027-8424, 1091-6490.

[65] Chen Xi Li et al. "MicroRNA-21 Preserves the Fibrotic Mechanical Memory of Mesenchymal Stem Cells". In: *Nature Materials* 16.3 (Mar. 2017), pp. 379–389. ISSN: 1476-1122, 1476-4660.

[66] Erica Hui, Kathryn I. Gimeno, Grant Guan, and Steven R. Caliari. "Spatiotemporal Control of Viscoelasticity in Phototunable Hyaluronic Acid Hydrogels". In: *Biomacromolecules* 20.11 (Nov. 11, 2019), pp. 4126–4134. ISSN: 1525-7797, 1526-4602.

[67] Jenna L. Sumey, Abigail M. Harrell, Peyton C. Johnston, and Steven R. Caliari. "Serial Passaging Affects Stromal Cell Mechanosensitivity on Hyaluronic Acid Hydrogels". In: *Macromolecular Bioscience* (Sept. 25, 2023), p. 2300110. ISSN: 1616-5187, 1616-5195.